



HAL
open science

Method Comparison for Fan Performance in Short Intake Nacelle

Alan Burlot, Fulvio Sartor, Maxime Vergez, Michaël Méheut, Raphaël Barrier

► **To cite this version:**

Alan Burlot, Fulvio Sartor, Maxime Vergez, Michaël Méheut, Raphaël Barrier. Method Comparison for Fan Performance in Short Intake Nacelle. 2018 Applied Aerodynamics Conference, Jun 2018, Atlanta, GA, United States. pp.4204, 10.2514/6.2018-4204 . hal-01924066

HAL Id: hal-01924066

<https://hal.science/hal-01924066>

Submitted on 14 Apr 2021

HAL is a multi-disciplinary open access archive for the deposit and dissemination of scientific research documents, whether they are published or not. The documents may come from teaching and research institutions in France or abroad, or from public or private research centers.

L'archive ouverte pluridisciplinaire **HAL**, est destinée au dépôt et à la diffusion de documents scientifiques de niveau recherche, publiés ou non, émanant des établissements d'enseignement et de recherche français ou étrangers, des laboratoires publics ou privés.



Method comparison for fan performance in short intake nacelle

A. Burlot¹, F. Sartor², M. Vergez³, M. Méheut⁴, R. Barrier⁵
ONERA, Université Paris Saclay, France

In order to evaluate the strong aerodynamic interactions between the secondary fan/*OGV* stage with the airframe engine integration system, and the ability of numerical methods to assess these interactions, several numerical methods have been tested. They range from RANS computation where the engine is modelled using simplified Boundary Conditions to full 360° URANS computations including the rotating fan blades. Intermediate methods such as Body-Force and Actuator Disk approaches have also been assessed. Computations were carried out on a generic configuration designed in the frame of the European ASPIRE project. The nacelle, short air intake and nozzle were designed by Airbus, the fan/*OGV* stage by DLR based on specifications provided by Airbus. This paper aims at presenting those results, including a grid convergence study, and at detailing the advantages and drawbacks of each method for two operating conditions: in cruise and at low speed.

Nomenclature

<i>ADP</i>	=	Aerodynamic Design Point
<i>LS</i>	=	Low-Speed
<i>URANS</i>	=	unsteady Reynolds Average Navier-Stokes
<i>AD</i>	=	Actuator-Disk
<i>BF</i>	=	Body-Force
<i>UP</i>	=	Uniform Pressure
<i>AB</i>	=	Abacus-based
<i>OGV</i>	=	Outlet Guide Vane
<i>FPR</i>	=	Fan Pressure Ratio
<i>BPR</i>	=	By-Pass Ratio
<i>RNA</i>	=	Blade number reduction (<i>Réduction du Nombre d'Aubes</i> in French)

I. Introduction

Environmental and energetic constraints are currently reshaping the aeronautical industry. The urge to reduce carbon-dioxide emissions and fuel consumption drives all actors to find new engine and aircraft designs. Among those, engines with increased by-pass ratio (*BPR*) appear to be the most valuable candidates for replacing the engines of existing aircrafts or short-terms programs (2025-2030 EIS). The *BPR* is the ratio between the mass flows passing through the secondary (cold) flux over the primary (hot) flux.

Reaching this high bypass ratio leads to a major modification in the nacelle and fan designs. In order to increase the flow in the secondary duct, the diameter of the nacelle must be increased. In the meantime, its length is reduced to limit the weight of the engine. This reduction leads to a diminution in the air intake length that allows stabilizing the flow in front of the fan blades. In that respect, the fan is subjected to more important flow fluctuations and distortions. More disruptive engine integration concepts can also lead to a more disturbed flow at the entrance of nacelle. For instance, one of the most studied alternatives is the partially buried engine with boundary layer ingestion.

Thus, all those new configurations call for a re-evaluation of design methods. The purpose of this paper is to compare the aerodynamic performance obtained with different numerical methods to model the fan/*OGV* stage. Two simplified methods are used: the actuator disk and the Body-Force methods. Those methods are compared with a complete 360° case using both *RANS* and *URANS* approaches. It shall allow identifying if intake/fan interactions prevent the use of simplified methods. All these activities were conducted in the frame of the European ASPIRE project in collaboration with Airbus, DLR and NLR.

¹ Dr., Research Engineer, *Aerodynamics, Aeroelasticity and Acoustics department*.

² Dr., Research Engineer, *Aerodynamics, Aeroelasticity and Acoustics department*, fulvio.sartor@onera.fr

³ Research Engineer, *Aerodynamics, Aeroelasticity and Acoustics department*, maxime.vergez@onera.fr

⁴ Dr., Research Engineer, *Aerodynamics, Aeroelasticity and Acoustics department*, michael.meheut@onera.fr

⁵ Research Engineer, *Aerodynamics, Aeroelasticity and Acoustics department*, raphael.barrier@onera.fr

A quick description of the different methods is given section II. The numerical specifications for all computations are described section III. Results and comparisons of the different approaches are presented in section IV with a focus on the overall values (mass flows, *FPR*, efficiencies), on radial and surface distributions.

II. Geometry and test-case definition

The configuration studied in this paper is a double-flux isolated nacelle including a UHBR engine (fan/*OGV* stage) as shown in Figure 1. This configuration was designed within the EU Clean Sky 2 research project ASPIRE as a generic engine for numerical studies, representative of future *UHBR* turbofan. The nacelle, air-intake and nozzle shapes were delivered by Airbus, while the fan/*OGV* blades were designed by DLR based on specifications provided by Airbus (including specifications for the core engine). It consists of 16 fan blades and 36 *OGV* blades. The nacelle features an air-inlet with a droop angle and a very small length-to-diameter ratio ($L/D \in [0.25; 0.35]$).

Nacelles with four different nozzles areas were designed to simulate a *UHBR* engine equipped with the Variable Area Nozzle Concept technology. In this paper, investigations focus on the aerodynamic performance at the Aerodynamic Design Point (*ADP*) and at Low-Speed (*LS*) (see Table 1).

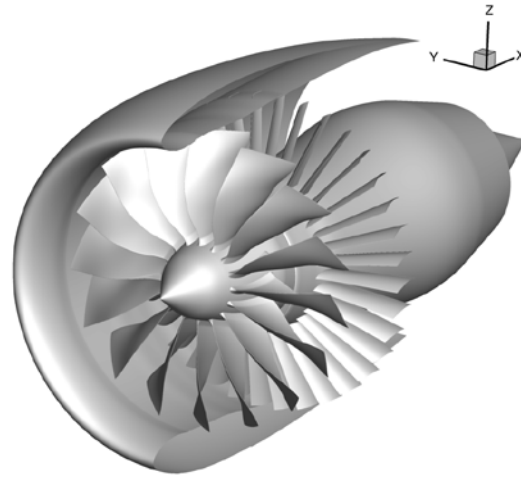


Figure 1 - ASPIRE Isolated UHBR Configuration

	Altitude [ft]	Mach Number (-)	Incidence angle (°)
Aerodynamic Design Point (<i>ADP</i>)	35,000	0.8	3
Low-Speed (<i>LS</i>)	0	0.3	15

Table 1 - Operating points.

III. Description of the methods

In order to obtain comparable and relevant results, a special mesh procedure was set-up to study the different fan modeling approaches (multi-block structured meshes):

- ✓ The nacelle is meshed independently with the ICEM- CFD software;
- ✓ The fan stage zone is left empty to be filled with a specific mesh for each case.

The fan air intake inner geometry at the fan station is axisymmetric unlike the upstream part of the air intake and of the nacelle. Due to the intake shortness, the fan leading edge exceeds the axisymmetric region. Thus, the surface separating the two domains needs to be curved. Details about the different methods are given below.

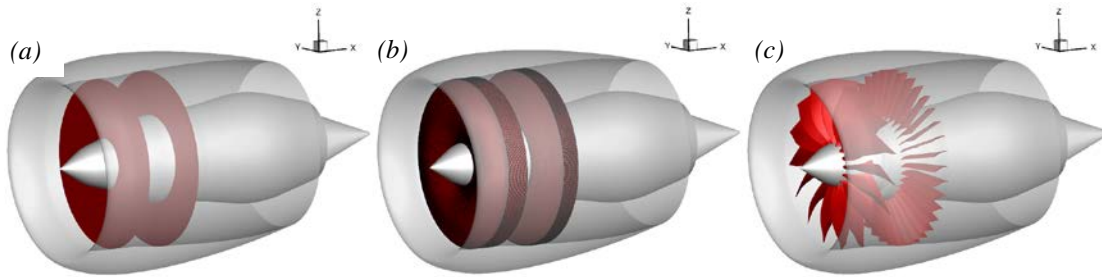


Figure 2 - Visualization of the three tested approaches: (a) nacelle with Actuator Disk; (b) nacelle with Body-Forces; (c) nacelle with all fan and OGV blades.

A. Actuator Disk (AD)

The purpose of using the *AD* is to reduce computational time as required in a pre-design stage, while having a realistic modeling of the fan stage. Two *AD* methods have been studied: the *AD* "Abacus-Based" and the *AD* "Uniform Pressure"

1. *AD* Abacus-based (*AD-AB*)

This method computes the required jumps to model the fan according to an abacus. This abacus contains pressure and temperature jumps as well as flow deviation angles. Two ways to define this data were studied:

- ✓ By providing RANS data of an isolated fan/*OGV* stage computation;
- ✓ By estimating the abacus with the Glauert method (originally designed for propellers) to provide a faster and a standalone method (meaning, independent from isolated fan/*OGV* computation).

With the first approach, the *AD* data are computed from isolated fan/*OGV* RANS computations. These computations enable to find the maximum efficiency of the fan which represents the condition that will be used to define the abacus.

The advantage of using the second approach is that the jumps can depend only on the radius and, in theory, on the upstream Mach number. As mentioned before, deviation of the flow can also be modeled (swirl) which requires in this case a second *AD* which will behave as an *OGV*. This *AD* will ensure that the swirl cancels out when crossing this second plane (see Figure 2 (b)). An example of the effect of this kind of *AD* method is shown in Figure 3 where the positions of both *ADs* are visible.

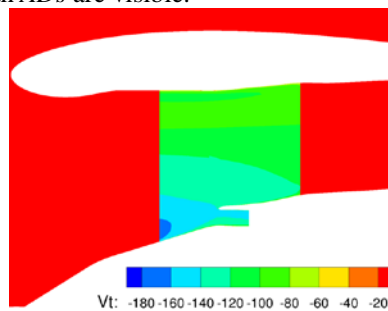


Figure 3 - Azimuthal velocity contour with the *AD-AB* approach.

With this *AD* method, the disk is decomposed into two boundary conditions, a prescribed mass flow outlet and the inlet is a prescribed P_i and H_i injection. This means that intrinsically, this *AD* formulation does not conserve the mass flow. Besides, since the upstream condition is an outlet condition, the upstream flow may not be influenced by the downstream flow compared to source terms methods.

The different tests made on these two approaches have shown that the first option was more reliable and accurate, so all results presented in this paper for the *AD* Abacus-based (*AD-AB*) are based on this approach.

2. *AD* Uniform Pressure (*AD-UP*)

This method is simpler than the previous one as it imposes a uniform pressure jump along the radius. This jump is applied to the flow with source terms so there is no discontinuity in the *CFD* domain compared to the *AD-UP*.

Figure 2 (a) shows the nacelle with the two actuator disks at the fan (front red plane) and *OGV* (rear red plane) blades locations.

B. Body-Force (*BF*)

The *BF* method consists in applying source terms to the *RANS* equations to model the effect of blades⁵. In this study, the *BF* method is used to model the fan and the *OGV* blades. Two models were first considered:

- ✓ The lift-drag model from Thollet⁷ which uses a *RANS* simulation of an isolated blade to calibrate the model;
- ✓ The modified Hall model⁶ which only requires the geometry of the blade.

If the blade geometry is not known, but if the flow characteristics in the vicinity of the blade are available, the lift-drag model can be used. On the opposite, if the blade geometry is known, it is possible to avoid the *RANS* computation by using the Hall model, which only needs the geometrical characteristics of the blades.

In the *ASPIRE* project, the blade geometry is known so the Hall model was used. With this model, the required blade characteristics are the following:

- ✓ Normalized position of the leading and the trailing edges;
- ✓ Blade chord taken along stream layers;
- ✓ Blockage factor;
- ✓ Gradient of the blockage factor with respect to the infinite flow direction (turbomachinery axis);
- ✓ Gradient of the blockage factor with respect to the radius;
- ✓ Normal to the skeleton along infinite flow direction, radius and azimuth;
- ✓ The tip clearance which corresponds to zero forces applied to the flow between the blade tip and the shroud

Figure 2 (b) shows the nacelle with the two Body-Force volumes at the fan (front red volume) and *OGV* (rear red volume) blades locations.

C. *RANS/URANS* 360°

Figure 2 (c) shows the complete 360° case which includes all engine components (fan, *OGV*, core, nacelle and nozzle). The fan and *OGV* meshes are obtained constructed using AutoGrid. One channel is meshed at first. Then, a duplication of this channel mesh is performed using the ONERA tool Cassiopée⁸ to obtain the complete 360° mesh.

Three interfaces between fixed and rotating parts must be specified using this approach:

- ✓ Between nacelle and fan domains in the air intake;
- ✓ Between fan and *OGV* domains;
- ✓ Between *OGV* and nacelle domains.

To perform *RANS* computations, a mixing plane boundary condition can be applied at these three interfaces: an azimuthal averaging is performed on the interface corresponding to the boundary and the averaged flow-field is transmitted from the upstream interface to the downstream one. For the *URANS* computations, an interpolation on the sliding mesh is performed in order to take into the account the unsteady effect. Figure 4 shows the impact of the methods on the pressure distributions through the fan/*OGV* stage. The difference between *RANS* and *URANS* is barely visible since the particular case of Figure 4 corresponds to a case with low angle of attack, where the flow is almost axisymmetric. However, *URANS* method with the sliding boundary condition is the only one capable of describing the interaction between the Fan and the *OGV* without performing spatial averaging. Due to the fact that the *RANS* equation are solved with a global time stepping, the results are also time accurate.

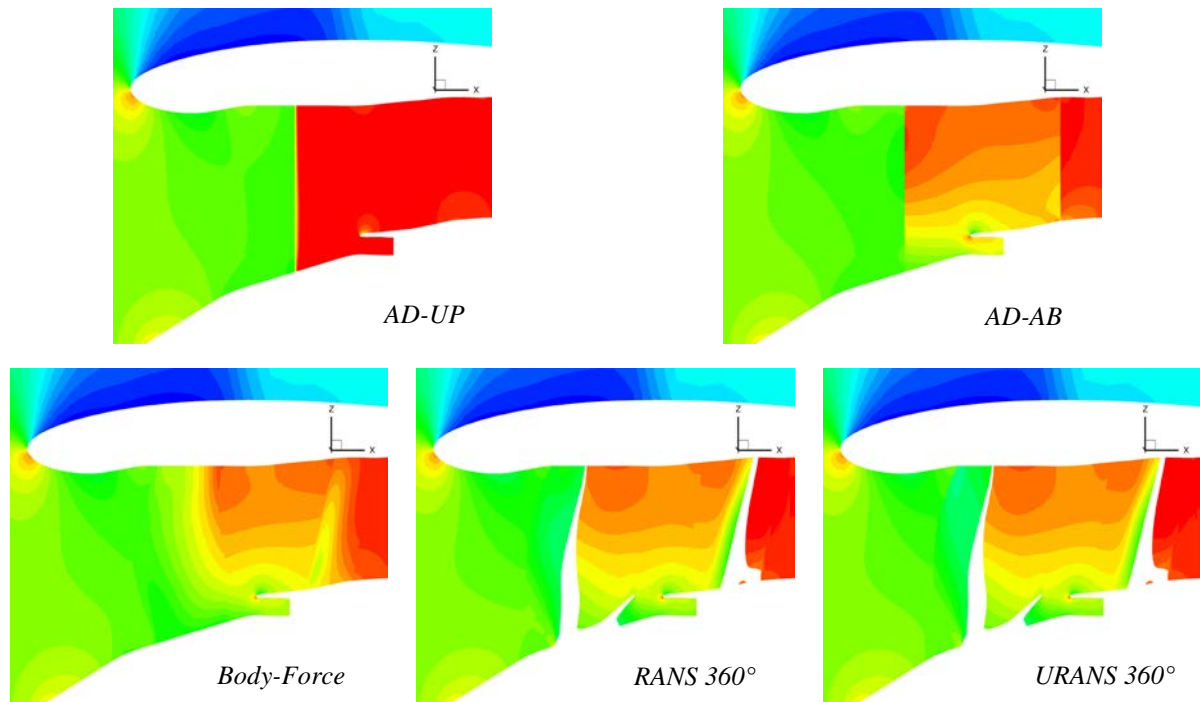


Figure 4 - Fan modelling with the different approaches (pressure distributions).

IV. Numerical setup

A. CFD code

All simulations were performed using the *elsA* solver⁹ (ONERA-Airbus-Safran property). The spatial numerical scheme is a cell-centered finite volume method with a Roe scheme. The steady solutions are obtained with an implicit backward Euler scheme. The turbulence model used is a Wilcox $k - \omega$.¹⁰

B. Grids

Three grid levels (coarse, medium and fine) were tested in order to assess the mesh convergence of the different approaches. The sizes of the different grids are detailed in Table 2. The medium grid was defined by coarsening the fine grid by a factor 2 in each direction. The same approach was applied to build the coarse grid from the medium one. The y^+ value was set at 1 for the medium case. The choice was made to have 60 points in the boundary layer on the fine grid to have an accurate description of the boundary layers. The 36 *OGV* meshes lead to a number of azimuthal points close to 1,200 which ensures to correctly capture the interactions between fan and *OGV* blades. The decision was made to restrain to 800 points in the same direction for the nacelle mesh to limit the total size of the mesh. The domain size has 10 chord-lengths for both upstream and downstream direction and 5 chord-lengths in the span-wise direction.

	<i>Coarse</i>	<i>Medium</i>	<i>Fine</i>
Nacelle	2.7 M	20 M	160 M
Actuator Disk	4.9 M	29 M	192 M
Body-Force	4.9 M	29 M	192 M
<i>RANS/URANS</i> 360°	4.2 M	32 M	247 M

Table 2 - Grid sizes (M: million of nodes).

C. Specific Boundary Conditions

A far-field boundary condition was applied on the external domain of the mesh where the following parameters are specified: Mach number, angle of attack, stagnation pressure and temperature.

The specific boundary conditions of each case (*ADP* and *LS*, see §II) were specified in the previous section. A valve condition was used in the *RANS* and *URANS* 360° and AD and BF computations that involve the primary outlet behind the fan. This condition allows reaching the correct mass flow by letting the static pressure fluctuate on the boundary condition.

V. Results

D. Global performance

Table 3 to Table 6 summarize some of the aerodynamic results obtained for both operating conditions (*ADP* and *LS*, 15, 20 and 25°). The results are presented in terms of differences with the specifications provided by Airbus for the three mass flows (fan, core and *OGV*) and the *FPR* for both conditions. For both efficiencies (fan, fan/*OGV* stage), the reference is the *URANS* computations performed on the medium grid (results on the fine grid are not available for all incidences at *LS*).

Table 3 and Table 4 show the results of the grid convergence study based on the *URANS* computations. Table 5 and Table 6 show the impact of the methods on the aerodynamic performance from results on the medium grid level.

Regarding grid convergence study, the results show that the difference between the *URANS* and the specifications progressively decreases with the grid size. This is especially the case for the total and secondary mass flows but also for the *FPR* which represent the most valuable performance for the fan (the core mass flow is really small compared to the secondary mass flow). It can also be noticed that the differences between the medium and fine grids are smaller than the ones between the coarse and medium grids, indicating a grid convergence.

At *ADP* conditions, the difference between the fine grid results and the specifications is lower than 0.1% for the three main aerodynamic characteristics (total, secondary mass flows and *FPR*). It is about 0.2 to 0.3% on the medium grid and about 0.5% for the coarse grid. At *LS*, the differences, even with the fine grid, are more important as expected. For the targeted incidence in the specifications (15°), the deviation is about 1.7% for the mass flows, smaller for the *FPR* (0.15%). As for *ADP*, the difference between the medium and fine grid levels is relatively small compared to the one between the coarse and medium grids. When the incidence (20 and 25°) increases, the mass flows and *FPR* decrease, with the same order of magnitude using coarse and medium grids.

As far as fan and *OGV* efficiencies are concerned, the results show that these efficiencies increase with the grid level (except at *ADP* for the total efficiency). This behavior can be correlated to the classical drag convergence study where the drag decreases with the grid size. The differences between the three grid levels are relatively significant especially between the coarse and medium grids (1 to 4% between the coarse and medium grids, about 0.5% between the medium and fine grids at *ADP*).

	ADP		
	Coarse	Medium	Fine
Fan Corrected Mass Flow	-0.27	0.31	0.11
Core Inlet Corrected Mass Flow	1.57	1.95	0.74
OGV Corrected Mass Flow	-0.35	0.19	0.09
Fan Pressure Ratio	-0.66	-0.05	-0.03
Fan Efficiency	-1.94	0.00	0.45
Fan + OGV Efficiency	-4.28	0.00	-0.44

Table 3 - LS - Aerodynamic fan performance for the URANS computations (in % compared to Airbus specifications for Mass Flow and FPR, compared to the URANS results on the medium grid for both efficiencies).

	LS 15°			LS 20°			LS 25°		
	Coarse	Medium	Fine	Coarse	Medium	Fine	Coarse	Medium	Fine
Fan Corrected Mass Flow	-2.27	-1.74	-1.69	-2.54	-1.97	-	-2.89	-2.33	-
Core Inlet Corrected Mass Flow	0.93	0.93	-0.71	0.99	0.75	-	1.03	0.21	-
OGV Corrected Mass Flow	-2.49	-1.99	-1.78	-2.80	-2.22	-	-3.18	-2.57	-
Fan Pressure Ratio	-0.39	-0.22	0.15	-0.51	-0.38	-	-0.66	-0.60	-
Fan Efficiency	-1.13	0.00	2.51	-0.96	0.00	-	-0.63	0.00	-
Fan + OGV Efficiency	-3.46	0.00	1.75	-3.41	0.00	-	-3.20	0.00	-

Table 4 - LS - Aerodynamic fan performance for the URANS computations (in % compared to Airbus specifications for Mass Flow and FPR, compared to the URANS results on the medium grid for both efficiencies).

In Table 5 and Table 6, the impact of the fan modeling methods can be seen on the fan performance. At *ADP*, the results with both *AD* approaches are available whereas at *LS*, only the results with *AD-UP* are available. This is due to the fact that the design of the abacus for *LS* was very difficult to achieve and the final results are not relevant.

At *ADP* and at *LS*, all methods provide mass flows values which are quite consistent; the maximum deviation between methods is about 1%. Regarding the *FPR* values, the gaps are even lower, the maximum deviation is about 0.6% for both operating conditions except for the *BF* approach where the deviation is about 1% at *ADP* and *LS*.

Regarding efficiencies, the results with the *AD-UP* approach show that this method is not able to predict fan and *OGV* efficiencies with a satisfactory accuracy. With this approach, these efficiencies depend on numerical

parameters which cannot be modified by the end-user. Since the *AD-UP* condition was initially designed for helicopter rotor applications, the imposed efficiencies are not adapted to fan/*OGV* applications. Looking at all other approaches, important deviations can also be observed. At *ADP*, with the *AD-AB* approach, the deviation is about 2% on the fan efficiency compared to *URANS* computations, about 1% with the *BF* method and 0.4% with *RANS* computations. At *LS*, the differences are more significant, about 6% with the *BF* approach and 2% with the *RANS* computations. These results clearly highlight that a better modeling of the fan enables to improve the accuracy for the fan and *OGV* efficiencies prediction (as far as *URANS* computations can be considered as the reference).

	ADP				
	AD UP	AD AB	BF	RANS	URANS
Fan Corrected Mass Flow	-0.40	0.56	-1.00	0.20	0.31
Core Inlet Corrected Mass Flow	0.00	0.01	0.01	-0.02	1.95
OGV Corrected Mass Flow	-0.43	0.38	-0.67	0.12	0.19
Fan Pressure Ratio	-0.02	-0.09	-1.08	-0.07	-0.05
Fan Efficiency	-14.06	-2.07	0.99	0.40	0.00
Fan + OGV Efficiency	-11.72	-2.66	1.39	0.10	0.00

Table 5 - ADP - Aerodynamic fan performance with the different approaches (in % compared to Airbus specifications for Mass Flow and FPR, compared to the URANS results on the medium grid for both efficiencies).

	LS 15°				LS 20°				LS 25°			
	AD UP	BF	RANS	URANS	AD UP	BF	RANS	URANS	AD UP	BF	RANS	URANS
Fan Corrected Mass Flow	-2.03	-1.44	-1.29	-1.74	-2.10	-1.67	-1.46	-1.97	-2.59	-2.03	-1.74	-2.33
Core Inlet Corrected Mass Flow	0.00	0.00	-0.03	0.93	0.00	0.00	-0.03	0.75	0.00	0.00	-0.03	0.21
OGV Corrected Mass Flow	-2.16	-1.13	-1.60	-1.99	-2.23	-1.37	-1.79	-2.22	-2.75	-1.76	-2.09	-2.57
Fan Pressure Ratio	-0.12	-0.42	0.05	-0.22	-0.12	-0.63	-0.03	-0.38	-0.26	-0.89	-0.13	-0.60
Fan Efficiency	-16.87	6.20	1.90	0.00	-17.48	6.48	2.32	0.00	-20.97	6.94	2.98	0.00
Fan + OGV Efficiency	-14.64	6.35	1.24	0.00	-15.59	6.16	1.49	0.00	-19.94	5.96	1.86	0.00

Table 6 - LS - Aerodynamic fan performance with the different approaches (in % compared to Airbus specifications for Mass Flow and FPR, compared to the URANS results on the medium grid for both efficiencies).

Figure 5 and Figure 6 give an overview of all results combining the grid convergence study and the different fan modeling approaches presented in this paper (respectively at *ADP* and *LS*). The left figures show the *FPR* vs. Corrected Mass Flow and right figures, the isentropic efficiency (fan/*OGV*) vs. the same mass flow.

These figures highlight that for all methods with the exception of the AD-AB, the grid refinement allows to get closer to the specifications, as expected. They also clearly evidence that both approaches using the complete geometry of fan and *OGV* blades provide more accurate results compared to the specifications. This is mainly the case at *ADP* (Figure 5), the differences with respect to the specifications in terms of mass flow are more significant at *LS* but the conclusions remain the same considering the different methods and the different grid levels.

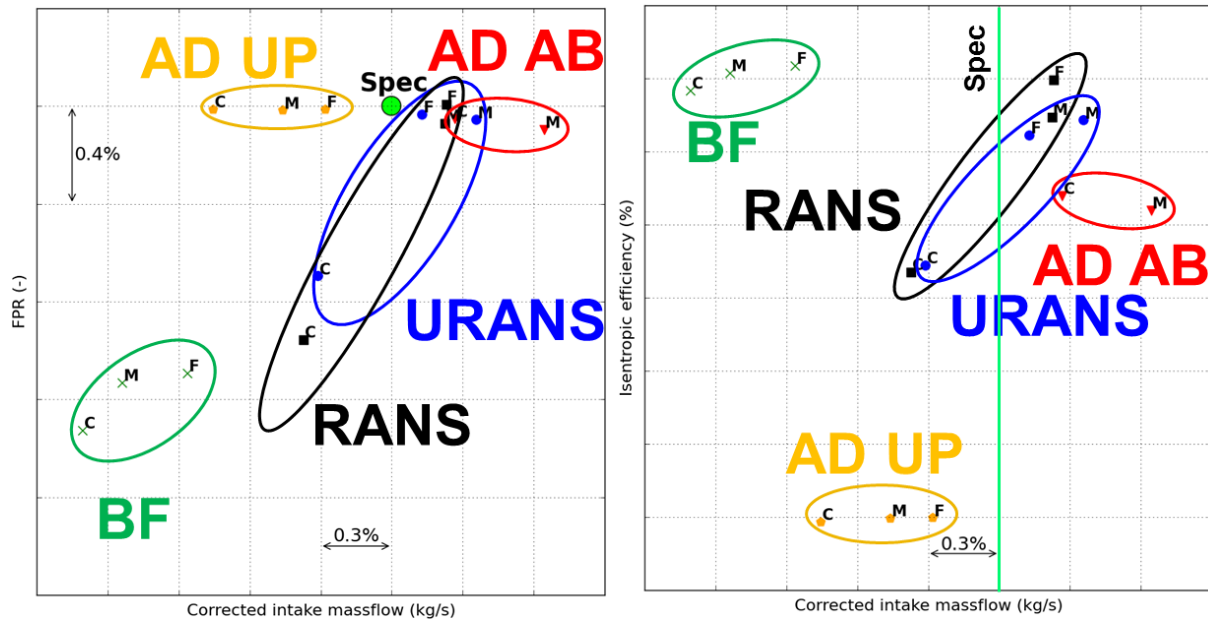


Figure 5 - *ADP* - *FPR* (left) and fan + *OGV* efficiency (right) versus Corrected Mass Flow for the three grid levels and the different fan modelling approaches (*C*: Coarse, *M*: medium, *F*: Fine).

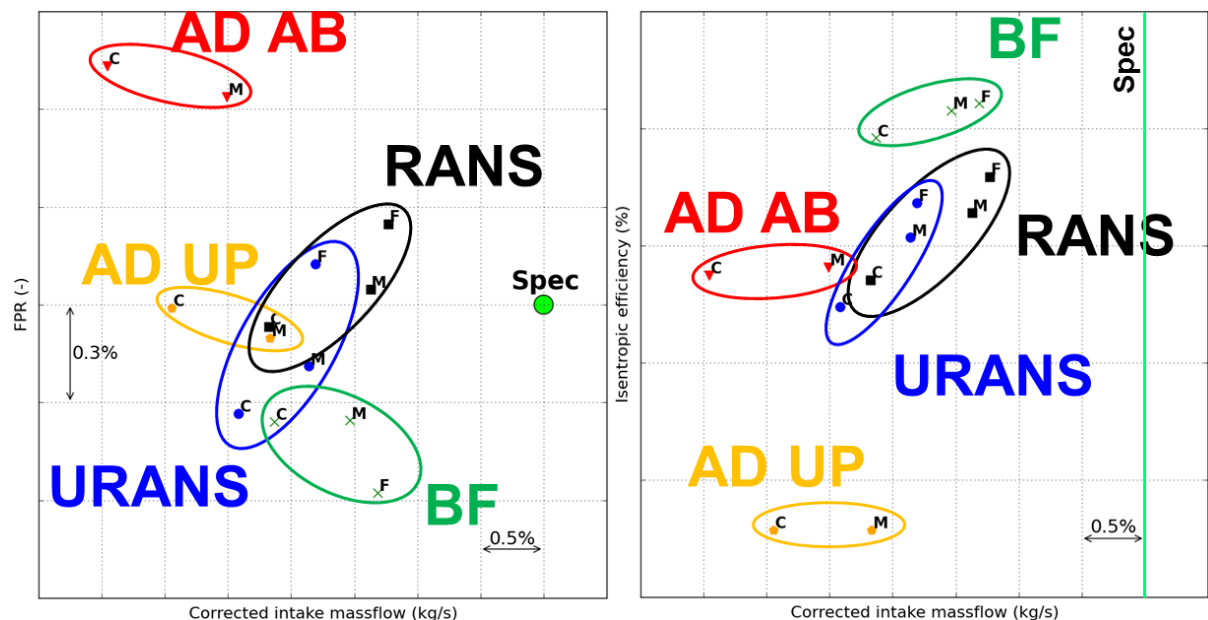


Figure 6 - *LS* - *FPR* (left) and fan + *OGV* efficiency (right) versus Corrected Mass Flow for the three grid levels and the different fan modelling approaches (*C*: Coarse, *M*: Medium, *F*: Fine).

E. Radial distributions

Figure 7 and Figure 8 show radial distribution of static and stagnation pressure downstream the *OGV* blades with the mesh refinement at both aerodynamic conditions. At *ADP* conditions, the static pressure levels are underestimated with the coarse grid compared to both medium and fine grid distributions. The stagnation pressure levels are underestimated for low radius values whereas near the blade tip, the pressure levels are equivalent with the grid levels.

At *LS*, the static pressure distributions are significantly different for the three grid levels whereas the stagnation pressure radial distributions are almost identical for the medium and fine grids. Concerning the coarse grid, the stagnation pressure level is underestimated near the hub but overestimated near the tip.

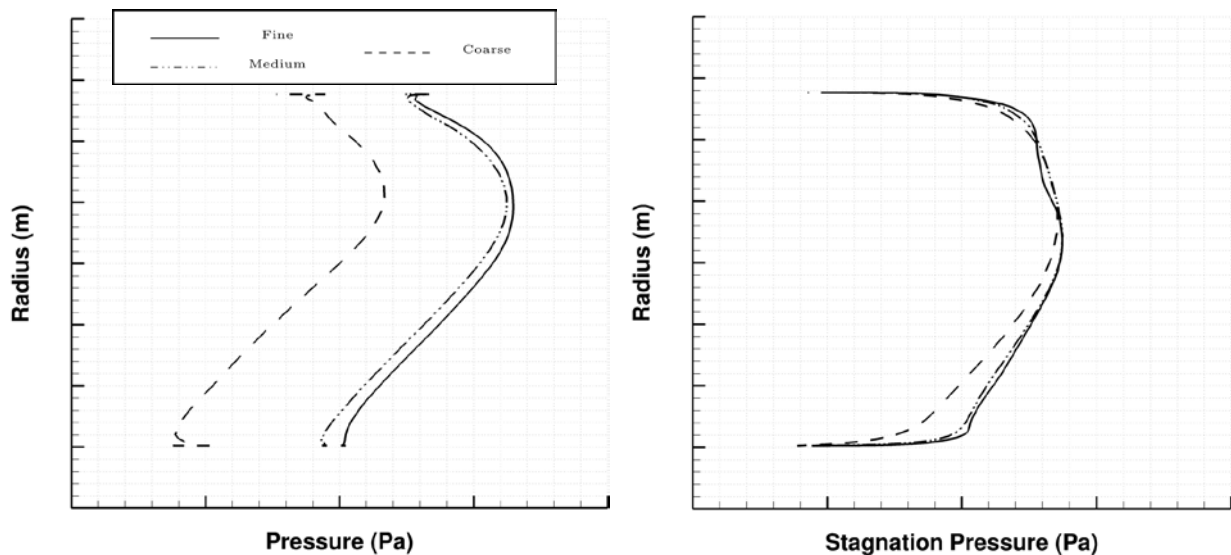


Figure 7 - *ADP* - Radial static (left) and stagnation (right) pressure distributions downstream of the *OGV* (right) for the three grid levels (*URANS* computations).

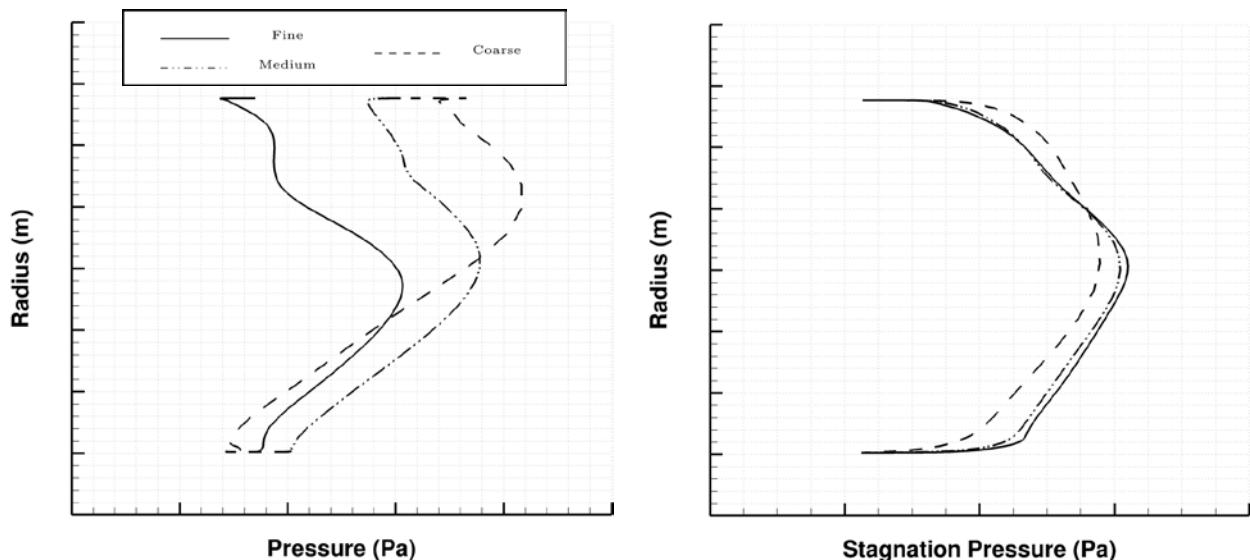


Figure 8 - *LS 15°* - Radial static (left) and stagnation (right) pressure distributions downstream of the *OGV* (right) for the three grid levels (*URANS* computations).

Figure 9 and Figure 10 show the impact of the fan modeling on the static and stagnation pressures radial distributions downstream of the *OGV* blades. The *RANS* and time-averaged *URANS* are very close to each other at *ADP*. At *LS*, the differences are significant in terms of static pressure but limited in terms of stagnation pressure. Only few deviations appear near the blade tip.

With both *AD* approaches, the static pressure levels are not accurately predicted, either overestimated (*AD-UP*) or underestimated (*AD-AB*) at *ADP* but also at *LS* with the *AD-UP* approach. With the *BF* method, the static pressure levels are underestimated at *ADP* and quite close to *RANS* results at *LS*.

As far as the stagnation pressure is concerned, the conclusions are slightly different. Indeed, with the *AD-UP* approach a uniform jump is imposed to the upstream flow through the fan which explains the shape of the orange curve in Figure 9 and Figure 10. Using the *AD-AB* approach in cruise enables to increase the accuracy of the stagnation pressure distributions at *ADP* but with some important deviations near the hub. With the *BF* method, the stagnation pressure levels are comparable on the first two-thirds of the blade radius at both conditions. Some discrepancies appear near the tip, mainly for the *ADP* case.

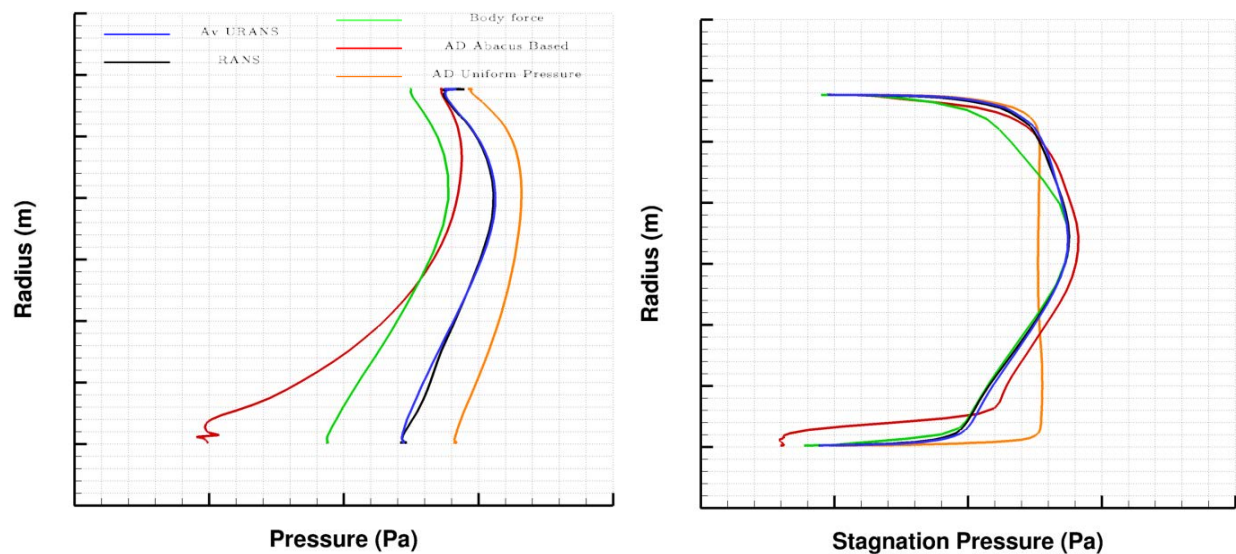


Figure 9 - *ADP* - Radial static (left) and stagnation (right) pressure distributions downstream of the *OGV* (right) for the different fan modelling approaches (Medium grid computations).

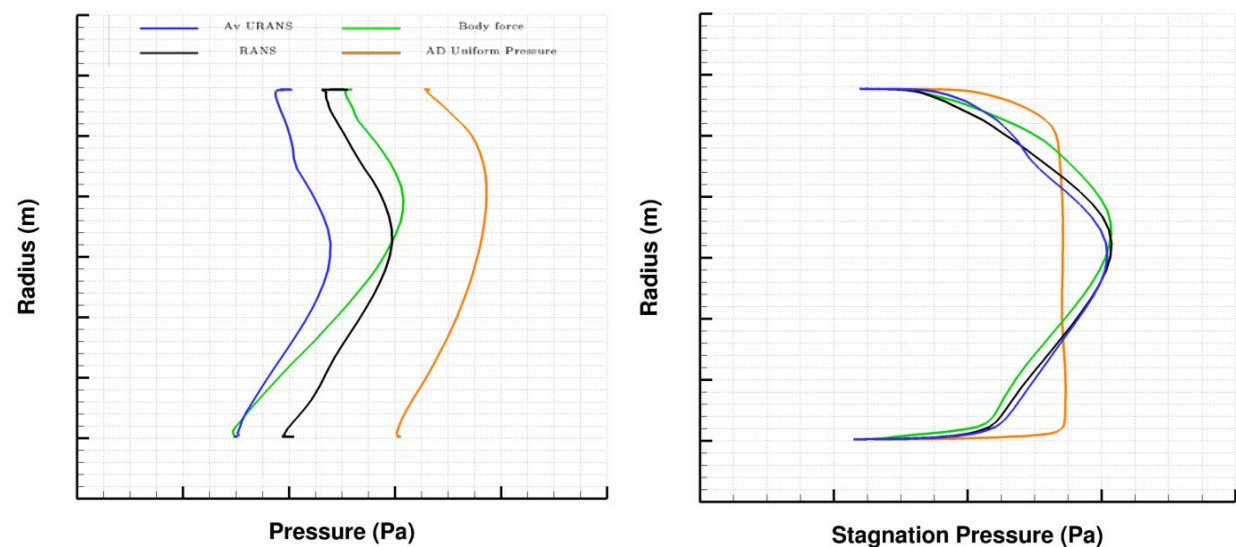


Figure 10 - *LS 15°* - Radial static (left) and stagnation (right) pressure distributions downstream of the *OGV* (right) for the different fan modelling approaches (Medium grid computations).

F. Stagnation pressure maps

Figure 11 to Figure 14 show stagnation pressure maps at two incidences (15 and 25°) at *LS* for the methods evaluated in this study. Figure 11 and Figure 13 show distributions upstream of the fan, Figure 12 and Figure 14, the same distributions downstream of the *OGV* blades.



Figure 11 - *LS* 15° - Stagnation Pressure maps upstream of the fan (left) for the different fan modelling approaches (Medium grid computations).

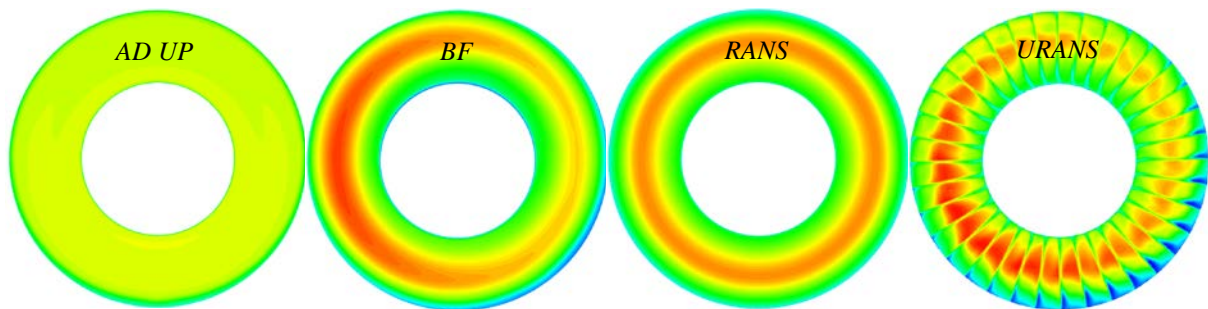


Figure 12 - *LS*15° - Stagnation Pressure maps downstream of the *OGV* (right) for the different fan modelling approaches (Medium grid computations).

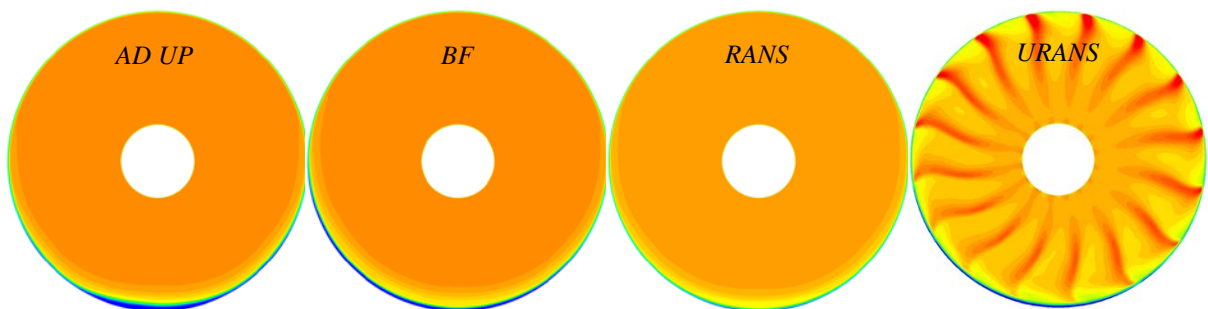


Figure 13 - *LS* 25° - Stagnation Pressure maps upstream of the fan (left) for the different fan modelling approaches (Medium grid computations).

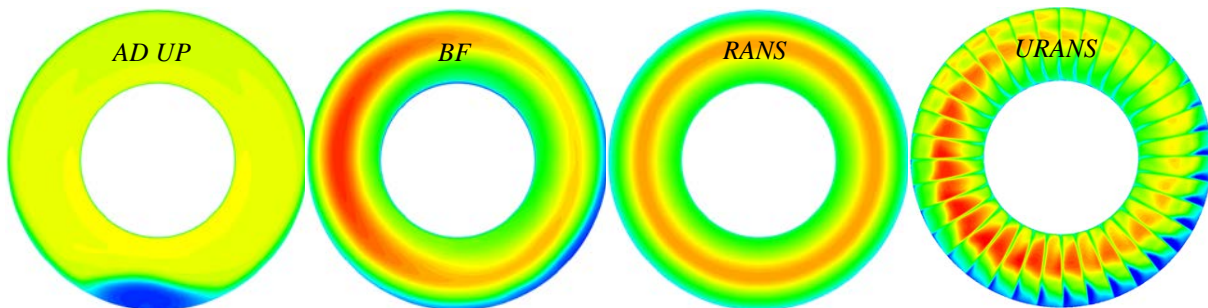


Figure 14 - *LS* 25° - Stagnation Pressure maps downstream of the *OGV* (right) for the different fan modelling approaches (Medium grid computations).

With all steady state methods (*AD*, *BF* and *RANS*), the stagnation pressure distributions does not represent the pressure variation due to the wake of the *OGV*. In the case of the 360° *RANS* computations, this is due to the use

of the mixing plane boundary condition between the fixed and rotating parts, which averages all azimuthal gradients and an axisymmetric distribution is thus obtained. This behavior presents a strong limitation in the case with high angle of attack: for example in the case at 25° , where the distortions created in the air inlet (see Figure 11) are averaged (and thus locally strongly reduced) along the azimuth downstream of the *OGV* blades. This means that all local flow separation that could occur at the bottom of the air inlet at high incidence angle would be diluted over the entire inlet.

The *AD* approach enables non axisymmetric distributions to be obtained but which remain quite far from the reference (*URANS* computations). At 25° of incidence, an important flow separation appears at the bottom of the air inlet whereas all other methods do not predict this separation in these conditions.

The distributions obtained with the *BF* methods are more relevant compared to the reference *URANS* computations. Indeed the high stagnation pressure levels observed on the left part of the *URANS* results are also predicted by the *BF* computations but with a small azimuthal deviation. This is also the case of the low stagnation pressure area at the bottom right of the figures.

The *URANS* distributions enable to visualize the unsteadiness of the flow and the local distortions seen by the fan and *OGV* blades. This is of great importance for the design of *UHBR* engine with very short inlet where the distortions are relatively high compared to existing engines.

G. Skin pressure distributions

Figure 15 to Figure 16 show the pressure distributions in the air inlet and on the fan/*OGV* blades for the three grid levels at both operating conditions. At *ADP*, the three distributions are globally equivalent but a detailed analysis of these distributions shows that the grid refinement enables to predict more accurately the weak shock waves near the fan blade tip or the pressure waves due to the blade passing in the air inlet. At *LS*, the same observations can be done, especially on the fan blade near the tip where the shock waves move upstream and are more intense with the increase of the grid size.

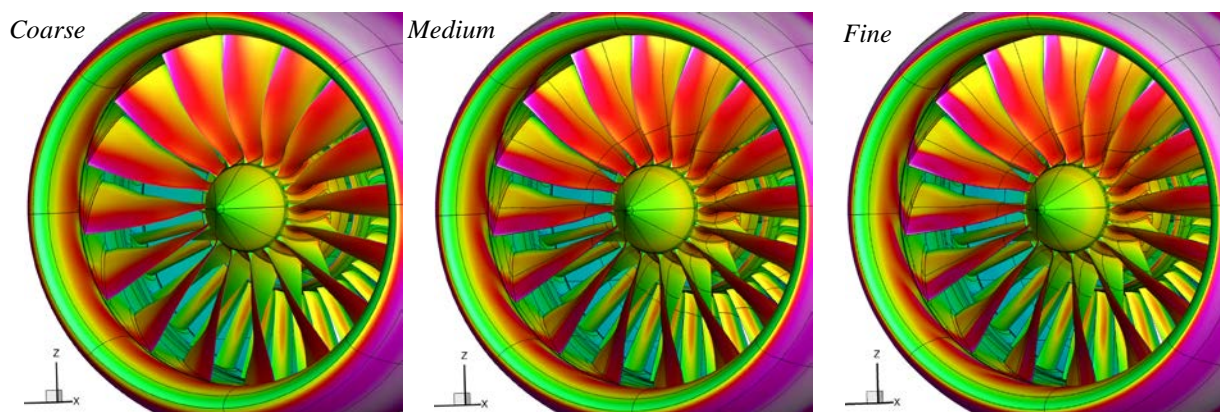


Figure 15 - *ADP* - Skin pressure distributions for the three grid levels (*URANS* computations).

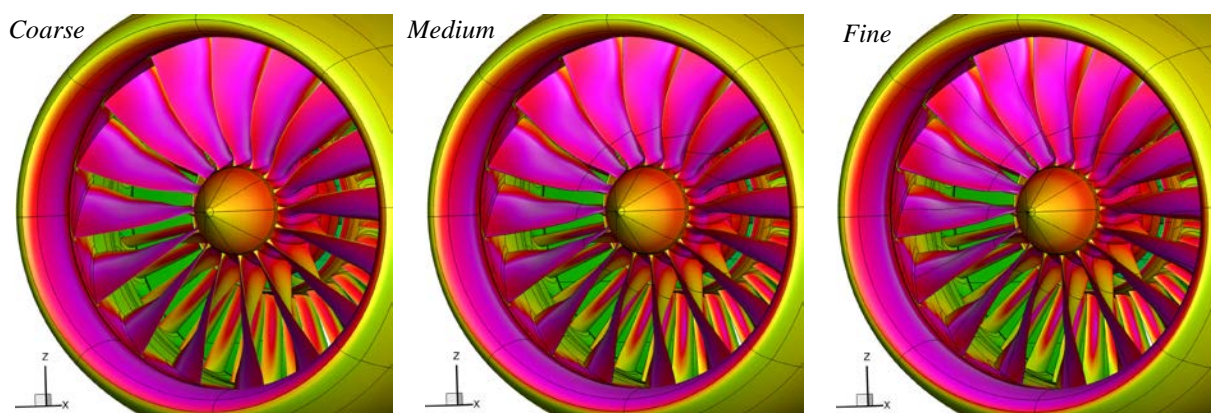


Figure 16 - *LS 15°* - Skin pressure distributions for the three grid levels (*URANS* computations).

Figure 17 to Figure 18 show the same pressure distributions on the medium grid for the different fan modeling methods at both operating conditions. With the *AD* approach, the distributions in the air inlet are, qualitatively

speaking, rather comparable to the *URANS* results but are completely different on the hub. This can be easily explained by the fact that the *AD-UP* method imposes a uniform pressure jump to model the fan which is not realistic in terms of radial pressure jump distributions as seen in Figure 9 and Figure 10.

With the *BF* approach, this pressure jump is more realistic which explains why the pressure distributions on the hub are closer to the results of the 360° *RANS* and *URANS* computations. With the *RANS* computations, the presence of the mixing planes implies that the pressure distributions are identical on all blades. This behavior is not realistic especially at *LS* conditions for high angles of attack where the loads on the fan blades are strongly dependent on their azimuthal positions. This also means that the fan passing is not visible on the air inlet pressure distributions.

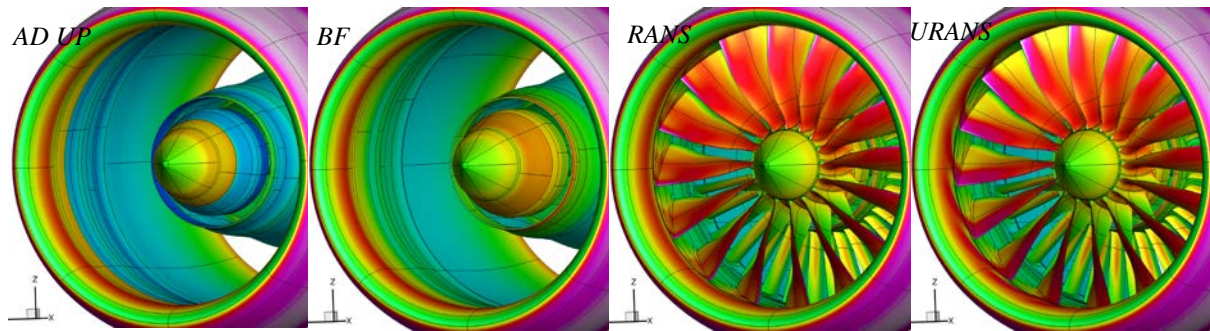


Figure 17 - ADP - Skin pressure distributions for the different fan modelling approaches (Medium grid computations).

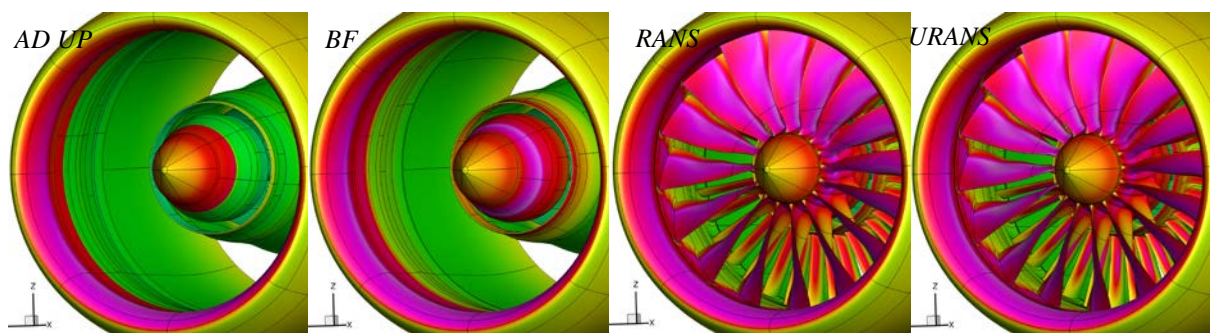


Figure 18 - LS 15° - Skin pressure distributions for the different fan modelling approaches (Medium grid computations).

VI. Conclusions

Different approaches to model the fan behavior in isolated nacelle computations were assessed in this paper. Two Actuator Disk approaches (with uniform pressure jump and based on an abacus) were tested together with the Body-Force technique which aims at modeling the fan and OGV blades with source terms to take into account the volume forces in the nacelle duct. The AD approaches impose surface discontinuities in the flow to model the fan and OGV blades. These methods were compared to 360° *RANS* and *URANS* computations where each fan and OGV blades are meshed to perform rotating fan computations in the isolated nacelle. Moreover, to draw more relevant conclusions, a grid convergence study was achieved for all methods with three grid levels (coarse, medium and fine). Two operating conditions were considered (in transonic cruise conditions and at take-off).

First, the results were presented in term of global values (mass flow, FPR and fan/OGV efficiencies). These results have shown that in cruise conditions, all methods are able to predict the primary and secondary mass flows with a deviation lower than 0.3% with the medium and fine grids compared to the specifications provided by Airbus. With the coarse grid, the deviation is about 0.6%. At low-speed, the differences are more significant, rising up to about 2% with the medium and fine grids and around 2.5% with the coarse grid. Regarding the Fan Pressure Ratio, the accuracy with respect to the specifications is about 0.1% in cruise and 0.3% at low-speed. Finally regarding fan and OGV efficiencies, the fan modeling methods and the grid size have a strong impact. Indeed, with the AD and BF approaches, the deviations are between 2 and 14% compared to the reference

URANS computations on the medium grid. The differences between RANS and URANS are rather small but the increase of the mesh size is really important especially between the coarse and medium levels (up to 4%).

Radial and surface distributions of static and stagnation pressure have also been compared. The results show that only the Body-Force approach is able to capture the main tendencies regarding the radial distributions but also the distortion maps downstream of the OGV blades. The 360° RANS computations provide relatively accurate results for the radial distributions but cannot correctly predict the distortion maps downstream of the OGV due to the azimuthal averaging of the flow using the mixing plane boundary condition. This is particularly the case for high incidence angles when separation occurs in the air inlet.

In conclusion, to correctly model the fan in terms of mass flow or FPR, simplified methods like the Body-Force can provide realistic results but 360° computations are required to have a good estimation of the fan and OGV efficiencies. With high distortion levels in the air inlet, the RANS computations are not able to correctly transfer these distortions through the fan and OGV stages, which could be critical in off-design conditions (at low-speed or in cross-wind conditions).

These computations were performed on an isolated configuration; the next step is to perform the same computations on an installed configuration to take into account the wing loading effect on the fan performance (configuration with underwing engine).

Acknowledgments

The studies presented in this article have used the ONERA-Airbus-SAFRAN *elsA* software whose development are partially funded by Airbus, Safran, and ONERA which are co-owners of this software.

This project has received funding from the Clean Sky 2 Joint Undertaking under the European Union's Horizon 2020 research and innovation program under grant agreement No 681856-2 - ASPIRE.



References

- ¹ Sabo, K. M. and Drela, M., "Benefits of Boundary Layer Ingestion Propulsion," *AIAA SciTech Forum*, American Institute of Aeronautics and Astronautics, Jan. 2015, pp. -.
- ² Peters, A., Spakovszky, Z. S., Lord, W. K., and Rose, B., "Ultrashort Nacelles for Low Fan Pressure Ratio Propulsors,"
- ³ *Journal of Turbomachinery*, Vol. 137, No. 2, Sept. 2014, pp. 021001-021001-14. Joo, W. G. and Hynes, T. P., "The Simulation of Turbomachinery Blade Rows in Asymmetric Flow Using Actuator Disks," *Journal of Turbomachinery*, Vol. 119, No. 4, Oct. 1997, pp. 723-732.
- ⁴ Wiat, L., Atinault, O., Boniface, J.-C., and Barrier, R., "Aeropropulsive Performance Analysis of the NOVA Configurations," *30th Congress of the International Council of the Aeronautical Sciences*, 2016.
- ⁵ Marble, F. E., "Three-Dimensional Flow in Turbomachineries," *High Speed Aerodynamics and Jet Propulsion*, Vol. 10, 1964, pp. 83-166.
- ⁶ Hall, D. K., *Analysis of civil aircraft propulsors with boundary layer ingestion*, Ph.D. thesis, Massachusetts Institute of Technology, 2015.
- ⁷ Thollet, W., *Body-Force modeling of fan-airframe interactions*, Ph.D. thesis, ISAE - Supaéro, 2017.
- ⁸ Benoit, B., Péron, S., and Landier, S., "Cassiopee: A CFD pre- and post-processing tool," *Aerospace Science and Technology*, Vol. 45, No. Supplement C, 2015, pp. 272 - 283. Cambier, L., Heib, S., and Plot, S., "The Onera elsA CFD software: input from research and feedback from industry," *Mechanics & Industry*, Vol. 14, No. 3, 2013, pp. 159-174.
- ⁹ Wilcox, D. C., "Reassessment of the scale-determining equation for advanced turbulence models," *AIAA Journal*, Vol. 26, No. 11, nov 1988, pp. 1299-1310.